Site preference and magnetic properties for a perpendicular recording material: $BaFe_{12-x}Zn_{x/2}Zr_{x/2}O_{19}$ nanoparticles

Z. W. Li,[1,*] C. K. Ong,[1] Z. Yang,[1,3] F. L. Wei,[3] X. Z. Zhou,[2] J. H. Zhao,[2] and A. H. Morrish[2]
[1]*Centre for Superconducting and Magnetic Materials and Department of Physics, National University of Singapore, Lower Kent Ridge Road, Singapore 119260*
[2]*Department of Physics, University of Manitoba, Winnipeg, Manitoba, Canada R3T 2N2*
[3]*Research Institute of Magnetic Materials, Lanzhou University, Lanzhou, People's Republic of China, 730000*
(Received 3 April 2000)

The site preference and magnetic properties of Zn-Zr substituted BaM ferrite $BaFe_{12-x}Zn_{x/2}Zr_{x/2}O_{19}$ nanoparticles with $x=0-1.6$ have been studied using Mössbauer spectra and magnetic measurement. The results show that the magnetizations and magnetocrystalline anisotropies are closely related to the distributions of Zn-Zr ions on the five sites. The $BaFe_{12-x}Zn_{x/2}Zr_{x/2}O_{19}$ nanoparticles exhibit unusual saturation magnetization, which increase at low substitutions, reach a maximum and then decrease. Mössbauer spectra show that the Zn-Zr ions preferentially occupy the $2b$ and $4f_{VI}$ sites. The preference for the $4f_{VI}$ site is responsible for the anomalous increase in the magnetization at low Zn-Zr substitutions. At $x \geqslant 1.2$ the rapid decrease in the magnetizations is mainly attributed to a noncollinear magnetic structure. In addition, a monotonic decrease in the magnetocrystalline anisotropy with Zn-Zr substitutions has its origin in the preference of the Zn-Zr ions for the $2b$ and $4f_{VI}$ sites.

I. INTRODUCTION

Fine BaM ferrite particles have attracted much attention during the last few years because of their applications in high density and perpendicular recording media.[1,2] For the various applications, a high saturation, a suitable coercivity and low-temperature coefficients of coercivity and remanence are desired. A lot of work has been done to modify the magnetic properties based on substitutions for Fe^{3+} ions with other ions. Among these, Co-Ti substituted BaM ferrites exhibit good properties; with increasing substitutions the saturation magnetization slightly decreases and the coercivity rapidly decreases from about 4.5 to 1 kOe.[3,4] However, these ferrites have a drawback, namely, a high-temperature coefficient of coercivity. This can be modified by adding a third element Sn^{4+} or by Ni-Zr substitutions.[5–7]

In the recent years we have focused our studies on Zn^{2+} substituted Ba ferrites. Zn-Ti (Ref. 8) or Zn-Sn (Ref. 9) substituted ferrite nanoparticles have been prepared by chemical coprecipitation, hydrothermal processes and synthesis from salt melts. Low cost Ba ferrite nanoparticles with a hexagonal and platelike crystals and a homogenous distributions of particle sizes can be obtained. The Zn-Ti and Zn-Sn substituted BaM ferrite nanoparticles exhibited interesting magnetic properties; the magnetizations have a smooth maximum at low substitutions and the coercivities have a significant change with substitutions. However, detailed studies on the origin of the unusual increase in the magnetizations and the rapid decrease in the coercivities are still lacking.

In this paper, substituted BaM ferrite nanoparticles $BaFe_{12-x}Zn_{x/2}Zr_{x/2}O_{19}$ are reported. The magnetic properties have been measured and Mössbauer spectra from 77 K to the Curie temperature have been collected and analyzed in an attempt to unravel the magnetic properties of these BaM ferrites on an atomic scale. Based on the distributions of the Zn-Zr ions on the five sites obtained from Mössbauer spectra, the origins of the unusual increase in magnetization and rapid decrease in coercivities are proposed. These results are also very useful for understanding the magnetic properties of other Zn^{2+} substituted BaM ferrites.

II. EXPERIMENT

The Zn-Zr substituted BaM ferrite nanoparticles $BaFe_{12-x}Zn_{x/2}Zr_{x/2}O_{19}$ with $x=0-1.6$, were prepared by a chemical coprecipitation. An aqueous solution of the metal chlorides containing Ba^{2+}, Fe^{3+}, Zn^{2+}, and Zr^{4+} in the ratio required for the ferrite was stirred in an excess of an aqueous solution of NaOH and Na_2CO_3. A suspension that is an intermediate precipitate was formed. Then, this product of coprecipitation was filtered and heated in air at an appropriate temperature. $BaFe_{12-x}Zn_{x/2}Zr_{x/2}O_{19}$ nanoparticles were obtained.

X-ray diffraction identified that all samples are single phases with the *M*-type hexagonal-ferrite structure. The apparent sizes $\varepsilon_F(110)$ and $\varepsilon_F(107)$ were determined from the widths of the broadening (110) and (107) x-ray lines, respectively. Then the average hexagonal diameter D and thickness t of particles were obtained based on the method proposed by Pernet *et al.*[10] The structure parameters and the sizes of particles are listed in Table I.

The magnetization curves of $BaFe_{12-x}Zn_{x/2}Zr_{x/2}O_{19}$ were measured in applied fields of 0–80 kOe and in a temperature range between 295 and 4.2 K using an extraction magnetometer made by the Quantum Design company. The coercivities were obtained from the demagnetization curves. Some intrinsic magnetic parameters, such as saturation magnetization M_s magnetic anisotropy field H_a and high-field susceptibility χ_p were deduced from a numerical analysis of the

TABLE I. Crystal structure parameters of $BaFe_{12-x}Zn_{x/2}Zr_{x/2}O_{19}$. Here, a and c are the lattice parameters, V is the cell volume, and D and t are the average diameter and thickness of nanoparticles, respectively.

x	a (nm)	c (nm)	c/a	V (nm^3)	D (nm)	t (nm)
0.2	0.589	2.317	3.934	0.696	93	38
0.4	0.590	2.324	3.939	0.700	73	34
0.6	0.590	2.325	3.941	0.701	74	32
0.8	0.590	2.326	3.942	0.701	75	28
1.0	0.590	2.331	3.951	0.703	71	27
1.2	0.591	2.338	3.957	0.707	65	26
1.6	0.591	2.344	3.966	0.709	49	25

magnetization curves based on the law of approach to saturation[11]

$$M(H)=M_s\left(1+\frac{A}{H}+\frac{B}{H^2}+\frac{C}{H^3}\right)+\chi_p H, \tag{1}$$

where $H=H_0-H_d$, H_0 is the applied field and H_d is the demagnetization field of the samples. The A/H term is related to the existence of inhomogeneities in the microcrystals and theoretically should vanish at high fields.[12,13] It was observed that the dependence of $M(H)$ on H is linear very well in high fields from 55 to 80 kOe and the second, third, and fourth terms in the bracket of Eq. (1) can be neglected. Hence, M_s and χ_p were obtained based on a linear least-squares method in the fields of 55–80 kOe.

The B/H^2 and C/H^3 terms are related to the magnetocrystalline anisotropy. For randomly oriented single domain particles without magnetic interactions between the particles B and C can be expressed as

$$B=-\frac{1}{15}H_a^2, \tag{2}$$

$$C=\frac{2}{105}H_a^3, \tag{3}$$

where H_a is the anisotropy field. For a uniaxial hexagonal compound with $K_2 \ll K_1$, H_a can be simplified as

$$H_a=\frac{2K_1}{M_s}. \tag{4}$$

It was found that in a range of the magnetic fields between 8 and 20 kOe, the A/H and χ_p terms in Eq. (1) can be neglected. The values of the anisotropy fields obtained from Eqs. (2) and (3) are close; the relative difference is less than 5% and the maximum difference is 8%. The value of H_a adopted in this paper is the average on the two values. Magnetocrystalline anisotropy constants, K_1, were calculated from Eq. (4).

Mössbauer absorbers were made by immobilizing the powdered samples in benzophenone for measurements below room temperature and in boron-nitride powders for high temperatures. All the absorbers contained about 4–5 mg/cm^2 of natural iron. Mössbauer spectra of $BaFe_{12-x}Zn_{x/2}Zr_{x/2}O_{19}$ were taken between 77 K and Curie temperature with a conventional constant-acceleration spectrometer. The γ-ray source was ^{57}Co in a Rh matrix. The calibration was made by using the spectrum of α-Fe.

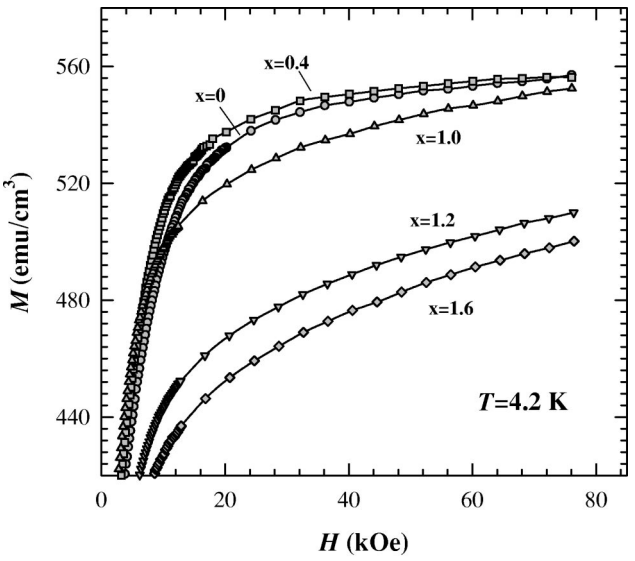

FIG. 1. Magnetization curves of $BaFe_{12-x}Zn_{x/2}Zr_{x/2}O_{19}$ with $x=0$, 0.4, 1.0, 1.2, and 1.6 at $T=4.2$ K.

Mössbauer spectra were analyzed using five sextets with Lorentzian line shape for the sample with $x=0$; they correspond to the five different crystallographic sites $4f_{VI}$, $2a$, $4f_{IV}$, $12k$, and $2b$, respectively. For the samples of $x>0$ the spectrum on the $12k$ sites may be decomposed into two or three subcomponents,[14] $12k$, $12k_1$, and $12k_2$, which corresponded to various Zn-Zr neighboring configurations at the $12k$ site. Some constraints were used in the fitting procedures. The area ratios of the six absorption lines in each sextet were assumed to be 3:2:1:1:2:3, because the absorbers were powders with randomly oriented particles. The area ratios among the sextets above Curie temperature were kept the same as those at room temperature. The corresponding linewidths for the $4f_{VI}$, $2a$, $4f_{IV}$, and $12k$ sites were constrained to be the same. However, the linewidths for the $2b$ site were about 30% larger than those for the other sites because of a peculiar diffusional motion of the Fe^{3+} ions within the trigonal bipyramid.[15] In addition, a relaxation sextet is observed at room temperature for the samples of $x \geqslant 0.8$.

III. RESULTS

A. Magnetic properties

The magnetization curves of $BaFe_{12-x}Zn_{x/2}Zr_{x/2}O_{19}$ with $x=0-1.6$ at $T=4.2$ K, as examples, are shown in Fig. 1. The specific saturation magnetizations σ_s, coercivities H_c, high-field susceptibilities χ_p, anisotropy fields H_a, and anisotropy constants K_1, obtained from the law of approach to saturation, are shown in Figs. 2–4.

Figure 2 shows the specific saturation magnetizations σ_s at $T=295$, 80, and 4.2 K as a function of Zn-Zr substitutions. The magnetizations exhibit two significant characteristics that are very different from Co-Ti and Co-Sn substituted barium ferrite. (1) With Zn-Zr substitutions, the values of σ_s increase at first and reach a smooth maximum at about

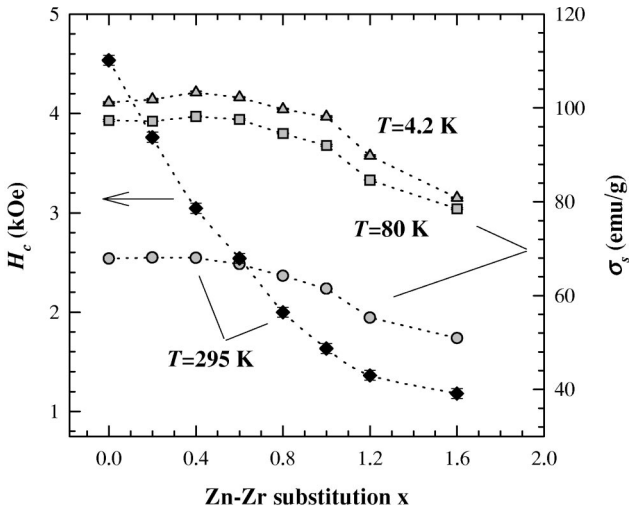

FIG. 2. Specific saturation magnetizations σ_s at $T=295$, 80, and 4.2 K and coercivities H_c $BaFe_{12-x}Zn_{x/2}Zr_{x/2}O_{19}$ at room temperature for $BaFe_{12-x}Zn_{x/2}Zr_{x/2}O_{19}$.

$x=0.4$ and 0.6. (2) At $x\geqslant 1.0$, the magnetizations rapidly reduce. Instead, the saturation magnetizations of the Co-Ti and Co-Sn substituted barium ferrite decrease monotonically and gradually.[16,17] These two characteristics will be discussed in detail in Sec. IV.

Figure 3 shows the high-field susceptibilities χ_p at $T=295$, 80, and 4.2 K as a function of Zn-Zr substitutions. The value of χ_p can be considered to be a constant to a good approximation in the substitution range from $x=0$ to 0.6 and increases slightly in a ranges from $x=1.2$ to 1.6. However, the value of χ_p rapidly increases from $x=0.6$ to $x=1.2$; the susceptibilities of the sample with $x=1.2$ are from double to fivefold larger than those of the sample with $x=0.6$. Similar results were also observed in $BaFe_{1-2x}Co_xTi_xO_{19}$.[18] The rapid increase in the high-field susceptibilities as well as the large decrease in the saturation magnetizations at $x=1.2$ to 1.6 suggest that a noncollinear magnetic structure (spin canting) occurs above $x\geqslant 1.2$.

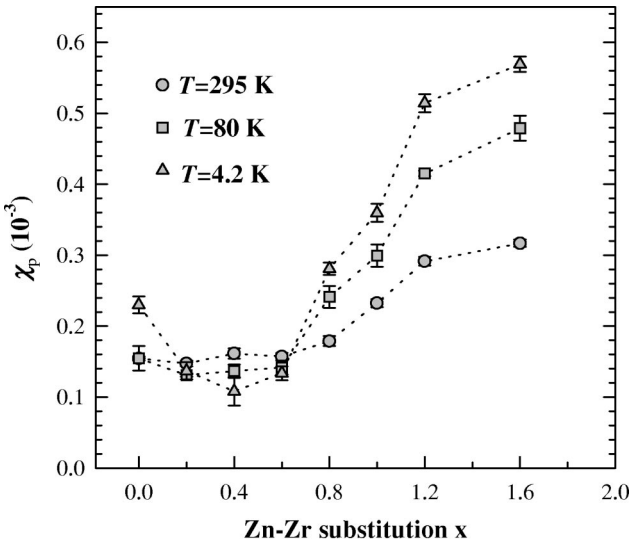

FIG. 3. High-field susceptibilities χ_p of $BaFe_{12-x}Zn_{x/2}Zr_{x/2}O_{19}$ at $T=295$, 80, and 4.2 K.

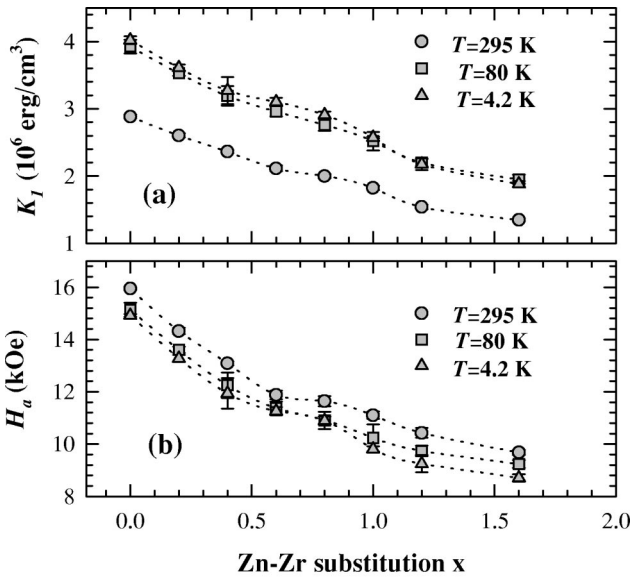

FIG. 4. (a) Magnetocrystalline anisotropy constant K_1 and (b) anisotropy field H_a of $BaFe_{12-x}Zn_{x/2}Zr_{x/2}O_{19}$ at $T=295$, 80, and 4.2 K.

Figures 4(a) and 4(b) show the magnetocrystalline anisotropy constants K_1 and the anisotropy fields H_a, respectively, at $T=295$, 80, and 4.2 K. With increasing Zn-Zr substitutions, a monotonic decrease in H_a and K_1 are observed. With decreasing temperatures, both the magnetizations and the magnetocrystalline anisotropy constants increase. However, the anisotropy fields decrease, because the magnetizations increase more rapidly than the anisotropy constants. Therefore, the anisotropy fields exhibit a positive temperature coefficient in a range between room temperature and 4.2 K for all the $BaFe_{12-x}Zn_{x/2}Zr_{x/2}O_{19}$ samples.

Figure 2 also shows the dependence of the coercivities on Zn-Zr substitutions at room temperature. The coercivities decrease almost linearly from 4.5 kOe for the sample with $x=0$ to 2 kOe for the sample with $x=0.8$. Therefore, for the Zn-Zr substituted BaM ferrite nanoparticles, the coercivities can be easily controlled from 4.5 to 2 kOe by adjusting the Zn-Zr substitutions and, at the same time, the saturation magnetizations are kept higher than or close to that for $BaFe_{12}O_{19}$.

B. Mössbauer spectra

Mössbauer spectra at room temperature together with the fitted subspectra for $BaFe_{12-x}Zn_{x/2}Zr_{x/2}O_{19}$ are shown in Fig. 5. The fitted Mössbauer parameters are shown in Figs. 6–8.

The average isomer shift $\langle\delta\rangle$ over the five sites as a function of Zn-Zr concentrations are shown in Fig. 6(a). With increasing Zn-Zr ions the isomer shifts decrease at first, reach a minimum at $x=0.8$ and then increase. This feature is attributed to two opposite factors. One is the decrease in the $3d$ moments of Fe ions with Zn-Zr substitutions and the other is the expansion of the cell volumes. The decrease in the moment of Fe^{3+} ions weakens the shielding effect of the $3d$ electrons on s electrons, which gives rise to an increment in the charge density at the nuclei. As a result, the isomer shifts will decrease. Whereas the expansion of the cell volumes leads to a decrease in the charge density at the nuclei.

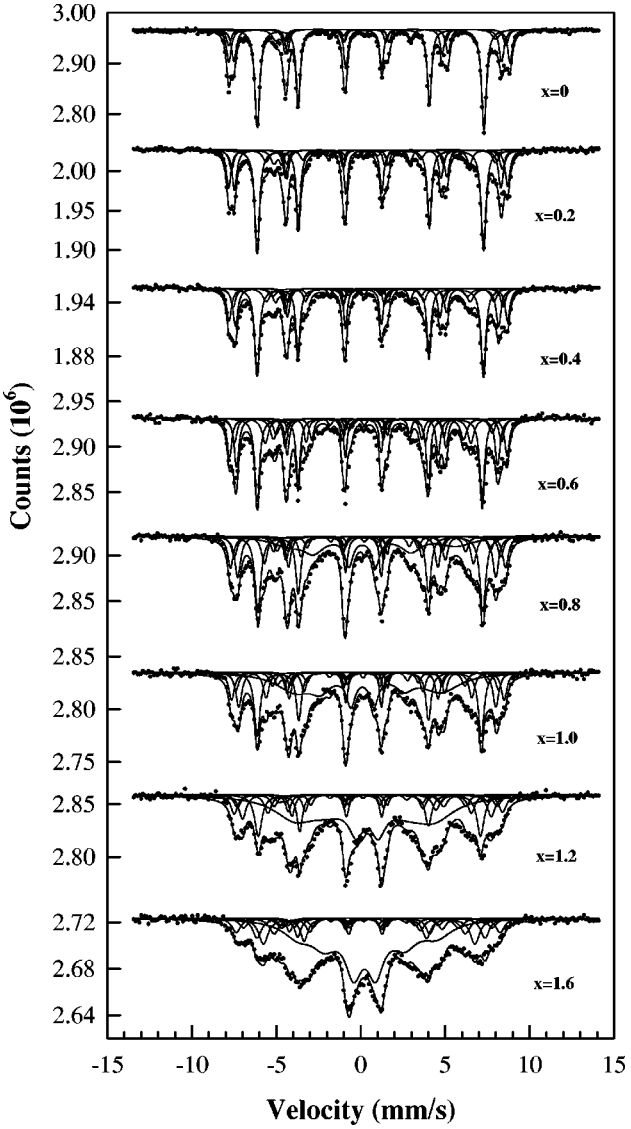

FIG. 5. Mössbauer spectra at room temperature for $BaFe_{12-x}Zn_{x/2}Zr_{x/2}O_{19}$ together with curves for the subspectra, obtained by a computer fit.

Hence, there is an increase in the isomer shifts. Quadrupole splitting, ϵ_{2b}, for the $2b$ sites and the average splitting $\langle\epsilon\rangle$ over the other four sites are shown in Fig. 6(b). A good linear relation between the quadrupole splittings and the Zn-Zr substitutions is observed.

Hyperfine fields on the five sites, as a function of the Zn-Zr substitutions, are shown in Fig. 7. The decrease in the hyperfine fields with the Zn-Zr substitutions is attributed to two factors. One is the decrease in the Fermi contact field produced by the polarization of Fe^{3+} ions. The other is the decrease in the super-transfer field that comes from the magnetic ions surrounding a given Fe^{3+} ion. The hyperfine fields can be considered to be linear to a good approximation within the experimental errors. The concentration coefficients of the hyperfine fields $dH_{\rm hf}/dx$ are listed in Table II. However, for the $4f_{\rm IV}$ site the fields deviate from the straight line at high Zn-Zr substitutions ($x=1.2$ and 1.6). The deviation may be related to the site occupation of Zn-Zr ions. It is known that for the $4f_{\rm IV}$ site there are three $12k$ sites as its nearest-neighbor and for other sites only one or two $12k$

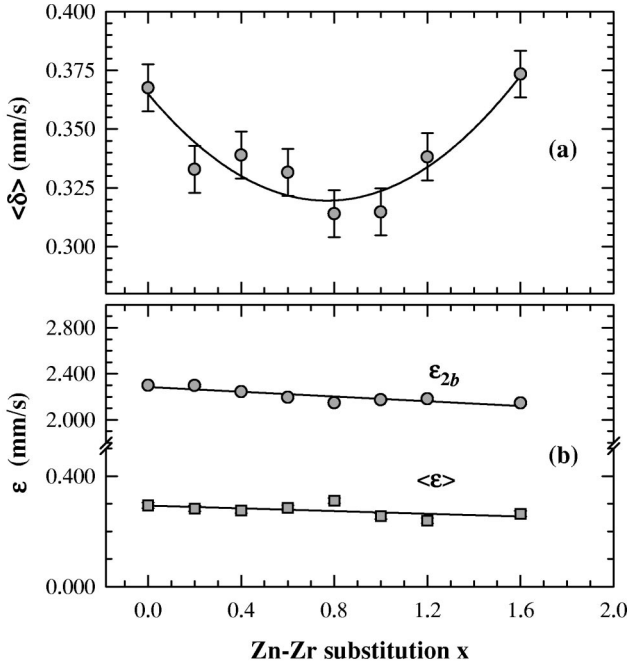

FIG. 6. Mössbauer parameters for $BaFe_{12-x}Zn_{x/2}Zr_{x/2}O_{19}$. $\langle\delta\rangle$ is the average isomer shift over the five sites; ϵ_{2b} and $\langle\epsilon\rangle$ are the quadrupole splitting for the $2b$ site and the average quadrupole splitting over the other four sites, respectively.

sites. Therefore, the Zn-Zr ions on the $12k$ site have stronger influence on hyperfine field for the $4f_{\rm IV}$ site than for the other sites. For the sample with $x>1.0$, the occupancy of Zn-Zr ions on the $12k$ site rapidly increases, from ~ 0 at $x<1.0$ to about 7%, at $x=1.6$, as shown in Fig. 8(b) or Fig. 9. This leads to a significant decrease in hyperfine field on the $4f_{\rm IV}$ site at high Zn-Zr substitutions.

A good fit was obtained for $BaFe_{12}O_{19}$ using five subspectra with relative area ratios of 2:1:2:6:1 corresponding to the $4f_{\rm VI}$, $2a$, $4f_{\rm IV}$, $12k$, and $2b$ sites. Therefore, it is reasonable to assume that the recoilless fractions on the five sites are the same. The relative areas, $S(i)$ $i=1-5$, of Mössbauer

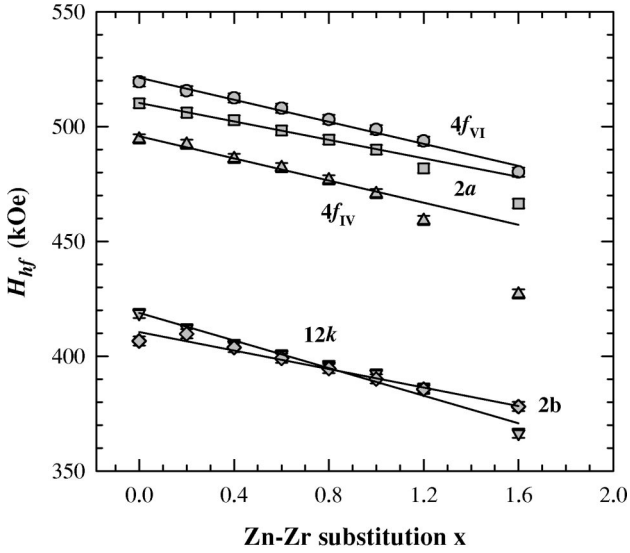

FIG. 7. Hyperfine fields $H_{\rm hf}$ on the five sites for $BaFe_{12-x}Zn_{x/2}Zr_{x/2}O_{19}$.

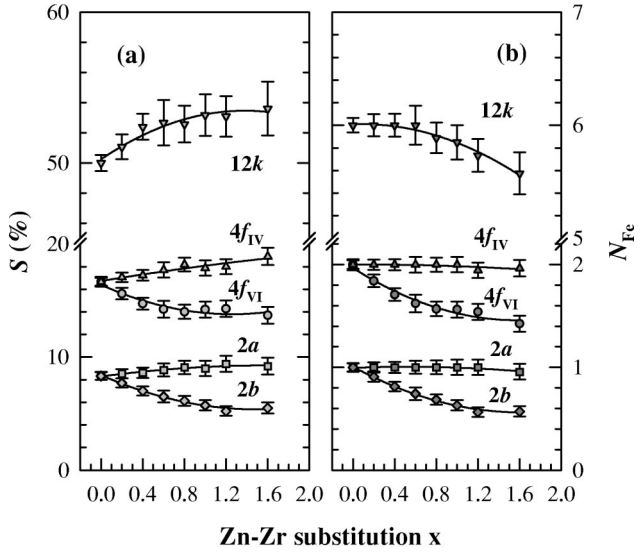

FIG. 8. The relative areas S_i of Mössbauer subspectra and (b) the occupation numbers $N_{\mathrm{Fe}}(i)$, of Fe ions on the five sites for $BaFe_{12-x}Zn_{x/2}Zr_{x/2}O_{19}$.

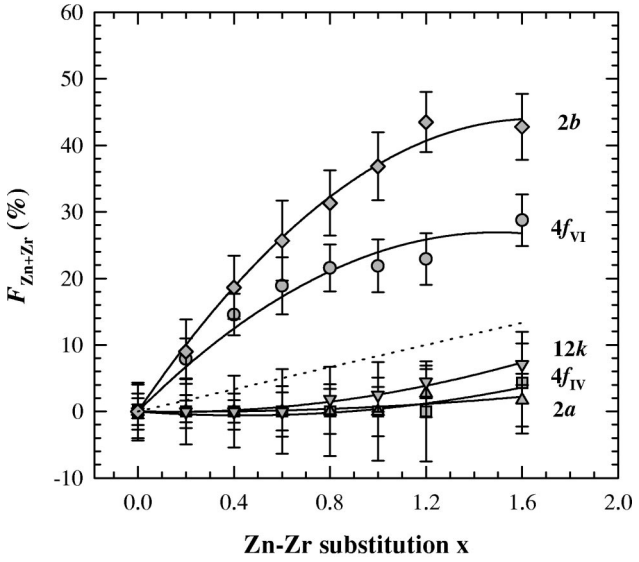

FIG. 9. Occupation fractions of Zn-Zr ions on each site for $BaFe_{12-x}Zn_{x/2}Zr_{x/2}O_{19}$ (the dotted line is for random occupancy by the Zn-Zr ions.)

subspectrum for the five sites are shown in Fig. 8(a). From these areas, the occupation numbers $N_{\mathrm{Fe}}(i)$ and $N_{\text{Zn-Zr}}(i)$, of Fe and Zn-Zr ions on the ith site can be estimated based on the formula

$$N_{\mathrm{Fe}}(i)=C_{Fe}\frac{S(i)}{\sum_{i=1}^{5}S(i)}, \tag{5}$$

$$N_{\text{Zn-Zr}}(i)=N(i)-N_{\mathrm{Fe}}(i), \tag{6}$$

where C_{Fe} denotes the compositions of the Fe ions and $N(i)$ is the occupation number for the ith site. The results are shown in Fig. 8(b). The occupancy fractions of Zn-Zr ions on the five sites

$$F_{\text{Zn-Zr}}(i)=N_{\text{Zn-Zr}}(i)/N(i)\times 100\% \tag{7}$$

are shown in Fig. 9.

In order to confirm the above results, some Mössbauer spectra were taken above Curie temperatures. These spectra consist of paramagnetic doublets. The quadrupole splitting is about 2 mm/s for the $2b$ site and is much larger than that for any other sites. As a result, for the $2b$ site, the subspectrum is separated from the other subspectra and an accurate subspectrum area can be obtained. In the fitting processes, the area ratios among the five subspectra were kept the same as those at room temperature. The fitted spectra are very well consistent with the experimental data, as shown in Fig. 10.

From Figs. 8(b) and 9, Zn-Zr ions preferentially occupy the $2b$ and $4f_{\mathrm{VI}}$ sites. The $12k$ site is involved in the substitutions at $x\geqslant 0.8$. The $4f_{\mathrm{IV}}$ and $2a$ sites seem not to be occupied by Zn-Zr ions from $x=0$ to $x=1.6$. The site occupancies are similar to the Co-Ti,[16,19] Co-Sn,[17] and Co-Mo[20] substitutions in BaM ferrite. Obradors *et al.*[21] have proposed that the $2b$ site can display a pseudotetrahedral character; hence, it is very possible for the Zn^{2+} ions to occupy the $2b$ site. Mössbauer spectra of $LaZnFe_{11}O_{19}$ showed that 90% of the Zn^{2+} ions are located on the site that has a maximum hyperfine field, i.e., the $4f_{\mathrm{VI}}$ site and the remaining Zn^{2+} ions occupy the $2b$ site.[22] Neutron diffraction of $BaFe_{1-2x}Zn_xTi_xO_{19}$ indicated that the Zn-Ti ions occupy the $4f_{\mathrm{VI}}$, $4f_{\mathrm{IV}}$, $12k$, and $2b$ sites, but exclude the $2a$ site in the low Zn-Ti substitutions.[23] In addition, the ions with a large radius, such as Sc^{3+} and In^{3+}, tend to occupy the $4f_{\mathrm{VI}}$ site;[24] whereas the Al^{3+} and Cr^{3+} ions have a small ionic radius and prefer the $2a$ and $4f_{\mathrm{IV}}$ sites.[25] Since the radii of both Zn^{2+} and Zr^{4+} ions are much larger than those of the Fe^{3+} ions, it is reasonable that the ions prefer the $4f_{\mathrm{VI}}$ site and exclude the $2a$ site.

In fact, the preference of Zn-Zr ions on the $4f_{\mathrm{VI}}$ site can be directly observed from Fig. 5. Let us notice the two Mössbauer lines at -7.5 and 8 mm/s. They are a summation of three subspectral lines corresponding to the $4f_{\mathrm{VI}}$, $2a$, and $4f_{\mathrm{IV}}$ sites. Obviously, in low Zn-Zr substitutions the shape of each of the two lines displays a considerable change; with increasing Zn-Zr, the relative intensities decrease for the outer subspectrum lines corresponding to the $4f_{\mathrm{VI}}$ site and increase for the inner lines corresponding to the $2a$ and $4f_{\mathrm{IV}}$ sites. This implies that the Zn-Zr ions prefer to occupy the $4f_{\mathrm{VI}}$ site.

At $x\geqslant 0.8$, there exists an extra sextet; it has broad linewidth and is not satisfied with the intensity ratios of

TABLE II. The concentration coefficient of hyperfine field dH_{hf}/dx, on each site for $BaFe_{12-x}Zn_{x/2}Zr_{x/2}O_{19}$.

Site	$4f_{\mathrm{VI}}$	$2a$	$4f_{\mathrm{IV}}$	$12k$	$2b$
dH_{hf}/dx (kOe)	$-23.9(12)$	$-20.1(4)$	$-24.1(13)$	$-30.1(20)$	$-20.2(15)$

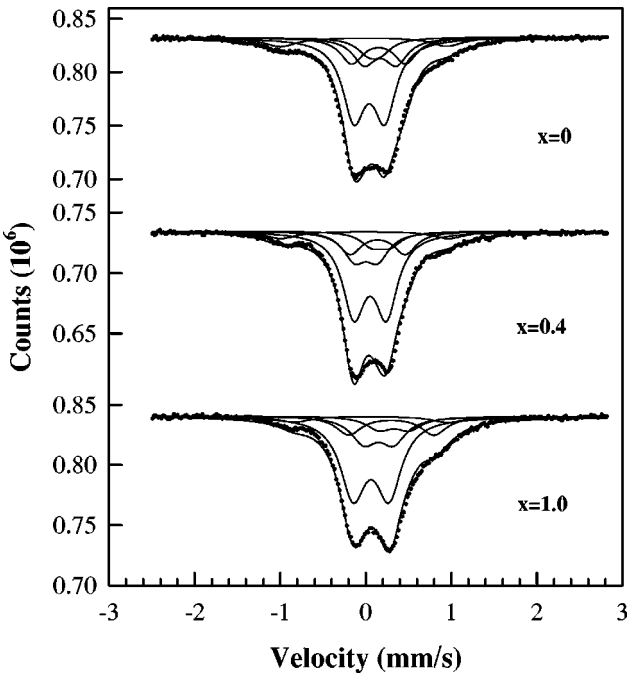

FIG. 10. Mössbauer spectra above Curie temperature for $BaFe_{12-x}Zn_{x/2}Zr_{x/2}O_{19}$ together with curves for the subspectra, obtained by a computer fit.

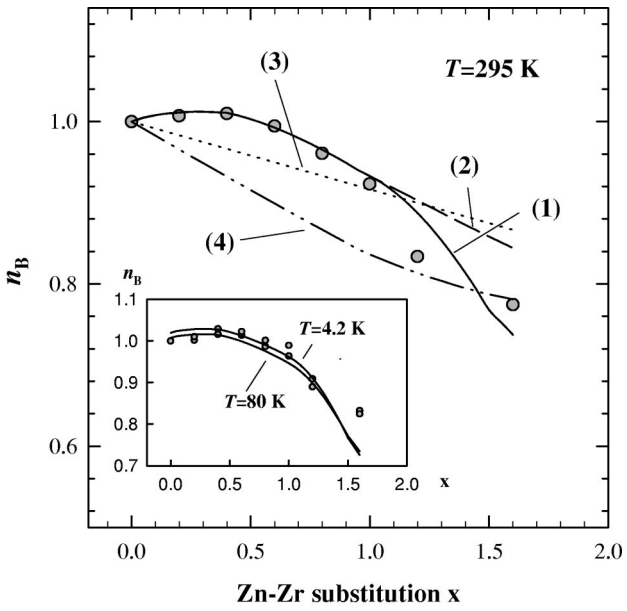

FIG. 11. The reduced number of Bohr magneton per chemical formula unit. (1) The solid line and (2) the dashed line are the values calculated by Eq. (8) for the noncollinear and collinear magnetic structures, respectively, (3) the dotted line is for the magnetic dilution model, and (4) the dash-dotted line is for the random-distribution model.

3:2:1:1:2:3 for the random oriented particles. The relative area of the sextet increase from 23% for the sample with $x=0.8$ to 50% for the sample with $x=1.6$. On the other hand, Mössbauer spectra show that with decreasing temperature, the areas reduce from 50% at room temperature to 12% at $T=77$ K for the sample with $x=1.6$. These features may be associated with a spin relaxation or superparamagnetic relaxation. The relaxations of nanoparticles in $BaFe_{12-x}Zn_{x/2}Zr_{x/2}O_{19}$ is very interesting problem that will be studied further.

IV. DISCUSSIONS

A. Site preference and magnetization

Zn-Zr substitutions in BaM ferrite lead to an abnormal increase in the magnetizations at low substitutions. However, the hyperfine fields on all five sites monotonically decrease in the whole range of substitutions. This excludes one possible origin that an enhancement in the moment of the Fe^{3+} ions produces the abnormal magnetizations.

As for a Zn spinel ferrite, the Zn-Zr ions in $BaFe_{12-x}Zn_{x/2}Zr_{x/2}O_{19}$ have two opposite influences on the magnetizations. It is known that, for a BaM ferrite, Fe^{3+} ions with up-spin are distributed on the $2a$, $12k$, and $2b$ site and ions with down-spin are located on the $4f_{IV}$ and $4f_{VI}$ sites. The Mössbauer spectra shows that the Zn-Zr ions preferentially occupy the $4f_{VI}$ site, as shown in Fig. 9, which makes a negative contribution to the magnetization. Consequently, the net magnetization increases. On the other hand, the Zn-Zr ions give rise to a decrease in the Fe moments (or hyperfine fields) on all sites, as shown in Fig. 7. As a result, the net magnetization decreases. Because of the competition between these two effects, the magnetization of $BaFe_{12-x}Zn_{x/2}Zr_{x/2}O_{19}$ exhibits an increase at first and then a decrease. A quantitative analysis of the magnetization is as follows.

Now the magnetizations or the number of Bohr magneton N_B per chemical formula unit or $BaFe_{12-x}Zn_{x/2}Zr_{x/2}O_{19}$ will be calculated based on the distributions of the Fe^{3+} ions on the five sites. Usually, an Fe magnetic moment is considered to be proportional to its hyperfine field. Therefore, the number of Bohr magnetons, N_B, can be obtained from the formula

$$N_B=\frac{1}{\alpha}\left(\sum_{i=1}^{3} H_{\mathrm{hf}}(i)N_{\mathrm{Fe}}(i)-\sum_{j=1}^{2} H_{\mathrm{hf}}(i)N_{\mathrm{Fe}}(j)\right), \qquad (8)$$

where i denotes the $2a$, $12k$, $2b$ sites, j the $4f_{VI}$ and $4f_{IV}$ sites and α is the proportionality coefficient between the Fe moment and the hyperfine field.

By substituting the hyperfine fields $H_{\mathrm{hf}}(i)$ and occupation numbers $N_{\mathrm{Fe}}(i)$ into Eq. (8), the number of Bohr magneton N_B as a function of Zn-Zr substitutions, can be calculated. For comparison between the calculated and experimental data, reduced values $n_B=N_B/N_B(0)$, are used; here $N_B(0)$ is the numbers of Bohr magneton for the sample with $x=0$. The results are shown by a dashed line in Fig. 11. The curve replicates the characteristics of the experimental data with low Zn-Zr concentrations; the numbers of Bohr magneton increase at first, reach a maximum and then decrease. However, at high substitutions, the calculated results have a larger deviation with the experimental values.

The high-field susceptibilities suggest a noncollinear magnetic structure at high substitutions of $x \geqslant 1.2$. The noncollinear structure has been confirmed for the Co-Ti substituted Ba ferrites based on Mössbauer spectra with a high field

applied parallel to the γ-ray direction.[26] Wartewig *et al.*[23] also indicated that for $BaFe_{12-2x}Zn_xTi_xO_{19}$ the canting angle mainly occurred in the 12*k* site and the value was about 25° in the applied field extrapolated to zero at $x=0.8$. Based on the noncollinear structure described by Wartewig, the value of the hyperfine field on the 12*k* site in Eq. (8) should be replaced by $H_{hf}\cos\theta$, where θ is the canting angle relative to the direction of an applied field. Then, it is assumed that the canting angles continuously change from 0° to 25° at the substitutions from $x=1.0$ and $x=1.6$. The reduced numbers of Bohr magneton n_B as a function of Zn-Zr substitutions, are calculated again from Eq. (8); the results are shown as the solid line of Fig. 11. The values agree very well with the experimental data in both low and high substitutions after the canting angles are introduced into the calculation.

As comparisons, two other models were used to calculate n_B. One is the magnetic dilution model. In this model, the moments of the Fe^{3+} ions are considered to be constant and the magnitudes of n_B only depend on the numbers of the Fe^{3+} ions. Obviously, the calculated n_B, as shown in the dotted line in Fig. 11, greatly deviates from the experimental data in both low and high substitutions. The other is the random-distribution model. In that model, Fe^{3+} ions are randomly distributed on all of the five sites. The reduced values of n_B calculated from the models are shown as the dot-dash lines in Fig. 11. The calculated results cannot show an increase in the magnetizations at low substitutions, although the results are consistent with the experimental values for the samples with $x=1.2$ and 1.6.

Similarly, the number of Bohr magnetons at $T=4.2$ and 80 K, plotted against the Zn-Zr substitutions, have also been calculated based on the distributions of the Fe^{3+} ions on the five sites and using the canting model. In the calculation, the following conditions are used. (1) The values of the hyperfine fields, 539 kOe for the $4f_{VI}$ site, 527 kOe for the 2*a*, $4f_{IV}$ and 12*k* sites and 440 kOe for the 2*b* site at $T=4.2$ K, and 533 kOe for the $4f_{VI}$ site, 514 kOe for the 2*a* and $4f_{IV}$ sites, 500 kOe for the 12*k* site, and 435 kOe for the 2*b* site at $T=80$ K, are taken from Refs. 27,28. (2) The dependences of the hyperfine fields on the Zn-Zr substitutions are kept the same as those at room temperature. (3) The canting angles are assumed to be the same as those at room temperature. The calculated results are shown in a inset of Fig. 11. The consistency between the calculated and experimental values shows again that the numbers of Bohr magneton per chemical formula or the magnetizations are closely related to the site preference of the Fe^{3+} ions and the noncollinear magnetic structure for $BaFe_{12-x}Zn_{x/2}Zr_{x/2}O_{19}$.

B. Site preference and magnetocrystalline anisotropy

It is known that the high magnetocrystalline anisotropy of BaM ferrites has its main origin in Fe^{3+} ions on the trigonal bipyramidal site, i.e., the 2*b* site, which has a large asymmetry because a ferric ion is surrounded by five oxygen ions. Fuchikami *et al.*[29] showed theoretically that the Fe^{3+} ions on the 2*b* site are principally responsible for the uniaxial anisotropy. Asti and Rinaldi[30] stressed that the contributions to the anisotropy from all of the five sites should be considered. Further, Xu *et al.*[31] calculated the magnetocrystalline anisotropy constants, $K_1^{cal}(i)$ $i=1-5$, on the five sites based on the single-ion model, as listed in Table III.

TABLE III. The values of K_1 for a single Fe^{3+} ion at each site for BaM ferrite by Ref. 31.

Site	$4f_{VI}$	2*a*	$4f_{IV}$	12*k*	2*b*
K_1 (cm^{-1}/ion)	0.51	0.23	0.18	−0.18	1.40

The single-ion model leads to two important conclusions: (1) Fe^{3+} ions on the 2*b* site provide the largest positive contribution to the magnetocrystalline anisotropy and (2) Fe^{3+} ions on the 12*k* site make a negative contribution. This implies that the total anisotropy constants are closely related to the occupancies of the Fe^{3+} ions, because the Zn and Zr ions are nonmagnetic and have no contribution to magnetocrystalline anisotropy. Based on the values of $K_1^{cal}(i)$ and the distributions $N_{Fe}(i)$, of Fe^{3+} ions on the five sites, the total anisotropy constant K_1^{cal} of $BaFe_{12-x}Zn_{x/2}Zr_{x/2}O_{19}$ can be calculated from

$$K_1^{cal}=\sum_{i=1}^{5} N_{Fe}(i)K_1^{cal}(i). \tag{9}$$

For comparison, both experiment and calculated values are reduced and then are plotted as a function of Zn-Zr substitutions, as shown by the solid line in Fig. 12. The reduced anisotropy constant is defined as $k_1=K_1/K_1(0)$ where $K_1(0)$ is the value for the sample with $x=0$. Figure 12 shows that the calculated values (solid line) are very consistent with the experimental results. However, if it is assumed that the Zn-Zr ions are randomly distributed on the five sites or only occupy the $4f_{VI}$ or 2*b* site, the values of k_1 calculated from Eq. (9) are shown by the dotted, dashed and dash-

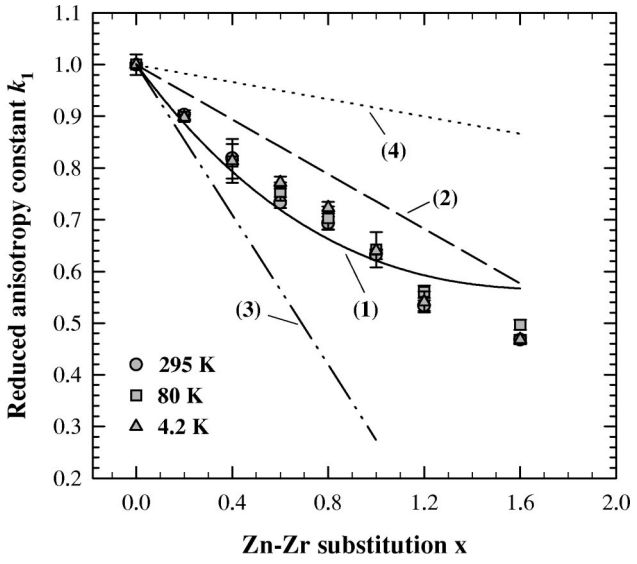

FIG. 12. Reduced magnetocrystalline anisotropy constants k_1. The symbols are the experimental data. The lines are for the values calculated from Eq. (9) based on the various distributions of Zn-Zr ions; for (1) the distributions of Zn-Zr ions are obtained from Mössbauer spectra, for (2) and (3) the Zn-Zr ions only occupy the $4f_{VI}$ and 2*b* sites, respectively, and for (4) the Zn-Zr ions are randomly located on the five sites.

dot lines, respectively, in Fig. 12. They are greatly deviated from the experimental data. Therefore, the change in the anisotropy constants with the substitutions is closely related to the site occupation of Fe^{3+} (or Zn-Zr) ions.

In addition, the dependences of the total anisotropy constants on the substitutions are almost the same in experimental errors at room temperature, 80 and 4.2 K. This implies that the temperature dependences of the anisotropy constants on each site are approximately the same, which agrees with the results of Xu *et al.*[31] Their calculation showed the temperature dependences are almost constant for the $2b$, $4f_{\mathrm{VI}}$, and $4f_{\mathrm{IV}}$ sites and are slightly larger for the $2a$ and $12k$ sites. However, it is known that the anisotropy contributions of the $12k$ and $2a$ sites are much less than those for the $2b$ and $4f_{\mathrm{VI}}$ sites.

Final, there is a considerable deviation between the experimental and calculated values at high substitutions of $x=1.2$ and 1.6. The approximation neglects the second order anisotropy constant in calculating the values of K_1 both from the single-ion model and from the law of approach to saturation. Possibly, for high Zn-Zr substitutions K_2 cannot be neglected.

V. CONCLUSIONS

The $BaFe_{12-x}Zn_{x/2}Zr_{x/2}O_{19}$ nanoparticles exhibit abnormal saturation magnetizations, which increase at low substitutions, reach a maximum at $x=0.4$ and then decrease at $T=295$, 80, and 4.2 K. The magnetocrystalline anisotropies, anisotropy fields and coercivities decrease rapidly and monotonously with Zn-Zr substitutions. The coercivities can be easily controlled from 4.5 to 2 kOe by adjusting the Zn-Zr substitutions and, at the same time, the saturation magnetizations are kept higher than or close to that for $BaFe_{12}O_{19}$.

The magnetizations and magnetocrystalline anisotropies are closely related to the distributions of the Zn-Zr ions on the five sites for $BaFe_{12-x}Zn_{x/2}Zr_{x/2}O_{19}$ nanoparticles. Mössbauer spectra shows that the Zn-Zr ions preferentially occupy the $2b$ and $4f_{\mathrm{VI}}$ sites. The preference on the $4f_{\mathrm{VI}}$ site is responsible for the increase in magnetizations at low Zn-Zr substitutions. At $x \geqslant 1.2$ the rapid decrease in the magnetizations is attributed to a noncollinear structure. A monotonic decrease in the magnetocrystalline anisotropies with the Zn-Zr substitutions has its origin in the preference of the Zn-Zr ions for the $2b$ and $4f_{\mathrm{VI}}$ sites.

*Email address: iesv6@nus.edu.sg

[1] D.E. Speliotis, IEEE Trans. Magn. **31**, 2877 (1995).
[2] T. Fujiwara, IEEE Trans. Magn. **21**, 1480 (1985).
[3] O. Kubo, T. Ido, and H. Yakoyama, IEEE Trans. Magn. **18**, 1122 (1982).
[4] Z. Yang, J.H. Zhao, H.X. Zeng, and G. Yan, Int. J. Soc. Mater. Eng. Resour. **3**, 203 (1995).
[5] O. Kubo, T. Nomura, T. Ido, and H. Yokoyama, IEEE Trans. Magn. **24**, 2859 (1988); O Kubo and E. Ogawa, *ibid.* **27**, 4657 (1991).
[6] Z. Yang, H.X. Zang, D.H. Han, J.Z. Liu, and S.L. Geng, J. Magn. Magn. Mater. **115**, 77 (1992).
[7] M.V. Rane, D. Bahadur, S.D. Kulkarni, and S.K. Date, J. Magn. Magn. Mater. **195**, L256 (1999).
[8] C.S. Wang, F.L. Wei, M. Lu, D.H. Han, and Z. Yang, J. Magn. Magn. Mater. **183**, 241 (1998); F.L. Wei, M. Lu, C.S. Wang, X.X. Liu, and Z. Yang, J. Magn. Soc. Jpn. **21**, 69 (1997).
[9] H.C. Fang, Z. Yang, C.K. Ong, Y Li, and C.S. Wang, J. Magn. Magn. Mater. **187**, 129 (1998); H.C. Fang, C.K. Ong, X.Y. Zhang, Y Li, X.Z. Wang, and Z. Yang, *ibid.* **191**, 241 (1999).
[10] M. Pernet, X. Obradors, M. Vallet, T. Hernandez, and P. Germi, IEEE Trans. Magn. **24**, 1898 (1988).
[11] R. Grossinger, Phys. Status Solidi A **66**, 665 (1981); J. Magn. Magn. Mater. **28**, 137 (1982).
[12] L. Néel, J. Phys. (France) **9**, 148 (1948); **9**, 193 (1948).
[13] A.T. Aldred and P.H. Froehle, Int. J. Magn. **2**, 195 (1972).
[14] G. Albanese, M. Carbuciccho, and G. Asti, J. Appl. Phys. **11**, 81 (1976); G. Albanese, A. Deriu, E. Lucchini, and G. Slokar, Appl. Phys. A: Solids Surf. **26**, 45 (1981).
[15] J.G. Rensen and J.S. van Wieringen, Solid State Commun. **7**, 1139 (1965); E. Kreber, U. Gonser, A. Trautwein, and F.E. Harris, J. Phys. Chem. Solids **36**, 263 (1975).
[16] X.Z. Zhou, A.H. Morrish, Z.W. Li, and Y.K. Hong, IEEE Trans. Magn. **27**, 4654 (1991).
[17] X.Z. Zhou, A.H. Morrish, Z. Yang, and H.X. Zeng, J. Appl. Phys. **75**, 5556 (1994).
[18] X. Batlle, X. Obradors, J. Rodriguez-Carvajal, M. Pernet, M.V. Cabanas, and M. Vallet, J. Appl. Phys. **70**, 1614 (1991).
[19] A.R. Corradi, D.E. Speliotis, A.H. Morrish, Q.A. Pankhurst, X.Z. Zhou, G. Bottoni, D. Candolfo, A. Cecchetti, and F. Masoli, IEEE Trans. Magn. **24**, 2862 (1988).
[20] D.G. Agresti, T.D. Shelfer, Y.K. Hong, and Y.J. Paig, IEEE Trans. Magn. **25**, 4069 (1989).
[21] X. Obradors, A. Collomb, M. Pernet, D. Samaras, and J.C. Joubert, J. Phys. Solid State Chem. **56**, 171 (1985).
[22] X. Obradors, A. Isalgue, A. Collomb, A. Labarta, M. Pernet, J.A. Pereda, J. Tejada, and J.C. Joubert, J. Phys. C **19**, 6605 (1986).
[23] P. Wartewig, M.K. Krause, P. Esquinazi, S. Rösler, and R. Sonntag, J. Magn. Magn. Mater. **192**, 83 (1999).
[24] G. Albanese, A. Deriu, E. Lucchini, and G. Slokar, Appl. Phys. A: Solids Surf. **26**, 45 (1981).
[25] G. Albanese, B.E. Watts, F. Leccabue, and S. Dìaz Castañòn, J. Magn. Magn. Mater. **184**, 337 (1998).
[26] K. Haneda, X. Z. Zhou, and A. H. Morrish (unpublished).
[27] K. Haneda and A.H. Morrish, IEEE Trans. Magn. **25**, 2597 (1989).
[28] J.S. van Wieringen, Philips Tech. Rev. **28**, 33 (1967).
[29] N. Fuchikami, J. Phys. Soc. Jpn. **34**, 760 (1965).
[30] G. Asti and S. Rinaldi, in *Magnetism and Magnetic Materials—1976*, edited by J.J. Becker and G.H. Lander, AIP Conf. Proc. No. 34 (AIP, New York, 1976), p. 214.
[31] Y. Xu, G.L. Yang, A.P. Chu, and H.R. Zhai, Phys. Status Solidi B **157**, 685 (1990).